P25 and its components – electronic properties and photocatalytic activities

Kunlei Wang,[a,b,*] Zhishun Wei,[c] Christophe Colbeau-Justin,[d] Akio Nitta,[a] Ewa Kowalska[a,*]

[a] Institute for Catalysis (ICAT), Hokkaido University, Sapporo, Japan

[b] Northwest Research Institute, Co. Ltd. of C.R.E.C., Lanzhou, China

[c] School of Materials and Chemical Engineering, Hubei University of Technology, Wuhan, China

[d] Laboratory of Physical Chemistry (LPC), Paris-Sud University, Orsay, France

*Correspondence: kunlei@cat.hokudai.ac.jp (K.W.) and kowalska@cat.hokudai.ac.jp (E.K)

Abstract

Photocatalytic activities and electronic properties of famous commercial photocatalyst – P25 has been investigated in detail. First, the active components have been isolated, i.e., anatase and rutile, characterized and tested. Although physical methods of phase separation are more recommended to keep original properties of polymorphs and to obtain the original amorphous phase, vibration and sonication-assisted vibration show to be ineffective for the phase separation. In contrast, chemical dissolution is effective, but resulting in impurification of titania surface, i.e., anatase with nitrogen and hydrogen peroxide, and rutile with fluorine. Therefore, purification methods must be applied, including thermal treatment and washing. Indeed, these post-treatment operations have resulted in preparation of almost pure anatase and rutile phases. However, annealing results in the particles' aggregation and might activate impurities adsorbed on the titania surface. Accordingly, the isolated rutile samples have additionally been washed with NaOH (to remove adsorbed HF) and then annealed. It has been confirmed that the high photocatalytic efficiency of P25 could be explained by the intrinsic properties of anatase and rutile, i.e., high activity in oxidation and reduction reactions, respectively. The mobility of charges and lifetime of electrons, studied by time-resolved microwave conductivity (TRMC), as well as density of electron traps, investigated by reverse double beam photoacoustic spectroscopy (RDB-PAS), allow to explain the common higher activity of anatase than rutile. Accordingly, it is thought that the higher activity of rutile for hydrogen evolution might be caused either by the more negative position of conduction band level or the more efficient light harvesting ability. Interestingly, the isolated samples have exhibited the visible-light response, especially those washed with NaOH and annealed, and thus suggesting that sodium (and/or its compounds), despite being not-recommended for UV activity, might initiate vis response of titania. At the same, it should be concluded that up to now the perfect method of isolation of active phases from P25 does not exist, as each method (even followed by purification) results in some changes in the composition and/or the surface properties of anatase, rutile and amorphous phase

Keywords

Evonik P25; phase separation; photocatalytic activity; charge mobility; electron lifetime; electron traps

1. Introduction

Heterogeneous photocatalysis has been intensively investigated for more than forty years, considering various aspects of environmental purification (water, wastewater, air, surfaces) and solar energy conversion into fuels and electricity [1,2]. Among various photocatalysts, titania is probably the most widely investigated and even commercially applied, including water treatment, and for "intelligent" surfaces with antimicrobial, self-cleaning and antifogging properties [3-6]. It has been proposed that for high photocatalytic activity, large specific surface area, high crystallinity and anatase polymorph are mainly recommended. However, it has also been found that commercial titania photocatalyst – P25 (mixed-phase titania: anatase>rutile>amorphous phase), despite not having the best surface properties, possesses the highest photocatalytic activity among different photocatalysts, and thus has commonly been used as a "standard material" for activity evaluation of various photocatalysts [7-19]. For example, P25 has exhibited very high activity in various reaction systems [20], such as: decomposition of organic [10,21-24] and inorganic [25] compounds, degradation of gas-phase pollutants [26-30], purification of indoor air [31], inactivation of microorganisms [17,32-34], self-cleaning surfaces [35-37], and solar energy conversion [38]. Various possible reasons of exceptional high activity of P25 have been proposed, including small particle sizes [39], large specific surface area [40], high crystallinity, co-existence of different polymorphs (anatase and rutile) [41-44], the presence of some impurities/dopants, such as Fe^{3+} [45] and/or the amorphous phase [46]. In 1991, Bickley et al. suggested that high activity of P25 (and other mixed-phase titania photocatalysts) was caused by the enhancement in "the magnitude of the space-charge potential" as a result of the contact between different phases and by the presence of localized electronic states in amorphous phase [46]. Commonly, the synergy (synergistic effect) has been applied for the explanation of high activity of P25, considering the interparticle charge transfer (IPCT) between phases (anatase-rutile), and thus inhibition of charge carriers' recombination [20,47-51]. However, usually there is no experimental evidence for the IPCT, which is speculated based on the results showing the higher activity of P25 than that of single titania phases (anatase and rutile). Moreover, in many cases, the activity of P25 has been only slightly higher than that of most active phase (usually anatase), but not higher than the simple sum of its parts (synergy), and thus even the term of "synergy" has been used incorrectly.

To confirm the "synergistic effect" (or/and IPCT), usually physical methods have been used, such as mixing and thermal treatment. The phase mixing can be performed either in the aqueous suspension of different titania particles under stirring or by the grinding of powder samples. The higher activity of the mixed-phase samples than that of sole anatase or rutile has been considered as a proof for

"synergistic effect". For example, Ohno et al. in 2003 reported the synergism between rutile and anatase in the photocatalytic oxidation of naphthalene for titania samples prepared by two methods: mixing of anatase and rutile and thermal treatment of anatase [52]. The synergetic effect was found in both kinds of samples (activity higher than the simple sum of its parts), and it was proposed that IPCT was responsible for this observation. Moreover, the activity of the most active mixed-phase titania was like that of P25. Based on these data, similar "synergy" was proposed for P25, i.e., electron transfer between anatase and rutile, resulting in its high photocatalytic activity.

Interestingly, Ohtani et al. have found that anatase and rutile, successfully isolated from P25 by chemical dissolution methods, are responsible for high photocatalytic activity in different reaction systems, i.e., oxidative decomposition of acetic acid and acetaldehyde in air, and oxygen liberation from a deaerated solution of aqueous silver sulfate, respectively [20]. Our recent study has also confirmed that anatase isolated from P25 is an active phase in oxidative decomposition of organic compounds, whereas rutile (also isolated from P25) for reductive pathway (methanol dehydrogenation) [53]. Therefore, the intrinsic properties of both phases (high activity for different reactions) could explain the exceptionally high activity of P25 in various systems without considering IPCT mechanism. Moreover, Ohtani et al. have confirmed that amorphous titania was almost inactive in all tested reactions. However, a commercial sample was used for this study since amorphous titania could not be isolated from P25 by chemical dissolution methods. Therefore, other methods, allowing physical separation of phases, have been tried in the present study to separate all components from P25, i.e., anatase, rutile and non-crystalline phase. Anyway, it is not expected that the influence of amorphous phase on the overall activity could be significant, due to its low content and negligible activity independently on the preparation procedure (large content of defects as charge carriers' recombination sites). Although P25 is composed of only one chemical compound – TiO_2, its polymorphs are different by particle size (smaller for anatase) and density (3.78 and 4.23 g cm^{-3} for anatase and rutile, respectively) [54-56], and thus it is expected that physical vibration might result in phase separation [57-60]. On the other hand, it should also be considered that vibration could result in the energy release, causing the aggregation due to the high friction between titania particles [61,62]. Moreover, it should be pointed out that also original amorphous titania could be isolated by physical methods.

Although it has been found that chemical dissolution methods, used for anatase and rutile isolation from P25, are efficient, the possibility of co-existence of some impurities on the surface of isolated phases (due to chemical etching) [53], which could participate in the overall photocatalytic activity, should be examined. Therefore, both the physical methods (vibration, sonication-assisted vibration) and the purification of phases after chemical separation have been investigated in this study.

2. Experimental part

2.1 Phase separation

2.1.1 Physical methods

Physical separation was carried out by two variants of vibration systems. In the first type of experiments, only a muscle massager (SHAKER HM-162, the frequency of ca. 20 Hz and amplitude of 1.5 mm) was used for the sample vibration, whereas in the second one, the additional sonication was applied. In brief, 1-kg portion of sample (original P25, without any treatment), supplied by Nippon Aerosil, was mechanically vibrated (from the bottom) in a plastic measuring cylinder with 18 sampling holes, localized at different positions from the cylinder bottom, as shown in **Fig. S1** (A-C). The samples were taken from different positions, e.g., vib. 1 means the first sampling hole from the bottom, as drawn in **Fig. S1** (A-B). In the case of second type of experiments, the sonication was used additionally (**Fig. S1** D) to avoid the aggregation of titania particles. An ultrasonication probe, supplied by SONICS & MATERIALS INC (VCX 130, the frequency of 20 kHz), was immersed inside P25 powder from the top part of the cylinder. The samples were taken from the top at different time for checking the crystalline composition.

2.1.2 Chemical isolation

It should be mentioned that P25, despite being used as a standard, is not uniform in the composition, and even samples taken from the same container but at different position (e.g., bottom vs top) show different properties, e.g., anatase, rutile and noncrystalline content could vary as follows: 76-80%, 13-15% and 6-11%, respectively [53]. Therefore, P25 was homogenized first, according to the procedure reported before [53]. In brief, original P25 (1 kg) was suspended in Milli-Q water (5 L) under mechanical stirring for 24 h and then dried by freeze-drying. The homogenized sample with uniform composition, i.e., 78 % anatase, 14 % rutile and 8 % noncrystalline phase [53], was named as HomoP25. Anatase particles were obtained from HomoP25 by selective dissolution of rutile phase in a hydrogen peroxide-ammonia mixture (H_2O_2-NH_3) under magnetic stirring for 15 h at 25 °C, as previously reported [53,63]. The residual titania was washed several times with Milli-Q water, centrifuged under 15,000 rpm, freeze dried, and named as iso-ana (isolated anatase). Post-treatment was applied to remove impurities, originated from the isolation process. Annealing in air was carried out at four different temperatures, i.e., 120 ºC, 200 ºC, 300 ºC and 500 ºC, in a rotary furnace for 2.5 h. The samples were named respectively to annealing temperature, e.g., [iso-ana-200] means the iso-ana sample annealed at 200 ºC.

Rutile particles were isolated from HomoP25 by selective dissolution of anatase phase in a diluted hydrofluoric acid (HF) solution under magnetic stirring for 24 h at room temperature, as was proposed by Ohno et al. in 2001 [64]. The residual titania was washed 5 times with Milli-Q water, centrifuged

(4,500 rpm), freeze dried, and named as iso-rut (isolated rutile). Similar to anatase samples, to remove the impurities originated from the isolation process, the post-annealing was applied using the same conditions, i.e., 2.5-h heating in a rotary furnace at 120 ºC, 200 ºC, 300 ºC and 500 ºC. The samples were named respectively to the annealing temperature, e.g., [iso-rut-300] means the iso-rut sample annealed at 300 ºC. In order to remove hydrofluoric acid from the surface of iso-rut and to avoid the formation of F-modified titania (during annealing), iso-rut was additionally washed with an aqueous solution of NaOH (1 M) under magnetic stirring for 30 min, then 5 times with water, and finally annealed. The samples were named respectively to the annealing temperature, such as iso-rut-NaOH-200 means the iso-rut sample washed with NaOH and annealed at 200 ºC.

2.2 Sample characterizations

Samples were characterized by various methods and techniques. The crystalline composition was investigated by X-ray diffraction (XRD) analysis on Rigaku Intelligent X-ray diffraction system SmartLab equipped with following parts: a sealed tube X-ray generator (a copper target; operated at 40 kV and 30 mA), a D/teX high-speed position sensitive detector system and an ASC-10 automatic sample changer. Analysis data acquisition conditions were as follows: range: 10-90°, scan speed: 1.00°/min and scan step: 0.008°. The obtained XRD patterns were analyzed by Rigaku PDXL, crystal structure analysis package including Rietveld analysis, installed in a computer controlling the diffractometer. The crystallinity of the samples was evaluated by the internal standard method, where highly crystalline nickel oxide (20.0 wt%) was used as a standard.

Absorption properties of samples were measured by diffuse reflectance spectroscopy (DRS), carried out on a spectrophotometer (Jasco V-670) equipped with a PIN-757 integrating sphere. The baseline was recorded using $BaSO_4$ as a reference.

The lifetimes of charge carriers (electrons) were estimated by time-resolved microwave conductivity (TRMC) method. The incident microwaves were generated by a Gunn diode of the Ka band and the tests were done at 36.8 GHz. The pulsed light source was a Nd: YAG laser providing IR radiation at a wavelength of 1064 nm. The full width at half maximum of one pulse was 10 ns, and the repetition frequency of the pulses was 10 Hz. UV light (355 nm) was obtained by tripling the IR radiation.

Reversed double-beam photoacoustic spectroscopy (RDB-PAS), was used for measuring the energy-resolved distribution of electron traps of titania powders. In RDB-PAS measurement, electrons in the valence band of a powder sample are directly excited to electron traps (ETs) and accumulate in the ETs from the deeper side (anodic) to the shallower side (cathodic) by wavelength-scanned continuous light, and an increase in photoabsorption of electron-filled ETs is measured by modulated light as a fix wavelength by PAS [65,66].

The morphology of samples was investigated by scanning transmission electron microscopy (STEM, Hitachi HD2000).

2.3 Photocatalytic activity tests

The photocatalytic activity tests were performed in 35-ml Pyrex test tubes under UV/vis ($\lambda > 290$ nm) irradiation with a 400-W high-pressure mercury arc lamp (Eiko-sha; emission spectra shown in previous study [67]) under magnetic stirring (ca. 500 rpm), while the temperature of the suspension during photoirradiation was maintained at 298 K in a thermostatically controlled water bath. The photocatalytic activities were examined in two reaction systems: oxidative decomposition of acetic acid (CO_2 system) and dehydrogenation of methanol (H_2 system). In the case of CO_2 system, photocatalytic activity was examined by measuring the amount of evolved carbon dioxide from continuously stirred suspensions of a sample (50 mg) in an aqueous solution of acetic acid (5.0 mL, 5.0 vol%). The sample tubes were sealed with rubber septa before irradiation. During irradiation, a portion (0.2 mL) of the gas phase was withdrawn from the testing tube with a syringe and subjected to gas chromatographic analysis (TCD-GC, Shimadzu GC-8A-IT). Whereas, in the case of H_2 system, platinum (Pt) was in-situ photodeposited on titania (Bare titania is almost inactive and co-catalyst, e.g., platinum, is necessary.). Similar conditions to CO_2 system were used, i.e., 50 mg of titania, 5 ml of solution (50 vol% of methanol) and sealing of testing tubes with rubber septa, but the reaction mixture was first pre-bubbled with argon to remove oxygen (electron scavenger) from the system. The activity was evaluated by measuring the amount of evolved H_2 by TCD-GC. The amount of photocatalyst (50 mg) was estimated experimentally in the previous studies to ensure the absorption of all photons for reliable comparison of different photocatalysts, as clarified by Kisch [68].

Visible-light activity was also analyzed for 2-propanol oxidative decomposition to acetone. The 50-mg sample was suspended in 2-propanol (5 vol%), the Pyrex tube was sealed with a rubber septum and irradiated in a photoreactor [69], equipped with Xe lamp, a cut-off filter ($\lambda > 450$ nm; spectral distribution shown previously [70]), a cold mirror and a water bath (298 K, thermostated) under continuous stirring. The samples were taken from the testing tube, filtrated via a syringeless filter, and analyzed by GC-FID (Shimadzu GC-14B) for acetone concentration.

3. Results and discussions

3.1 Physical separation

First, the vibration was used to separate titania components from original P25 sample. However, 24-h vibration hardly changed the P25 composition, as almost same data were obtained for the samples taken at different sampling positions of the cylinder (vib.1 to vib.5), as shown in **Fig. S1** F. Interestingly, it has been found that the volume of the sample has decreased significantly during the vibration (first 1000 min), which could be caused by the aggregation of particles. Indeed, the large aggregates, i.e., the balls of a few mm, were formed, as shown in **Fig. S2** A-B. It has been reported that, during mechanic vibration, the vibration energy could be transfer to the particles, causing their easy aggregation by van der Waals force between particles [61,62]. During the further long-term vibration (>

1000 min), the volume did not change, suggesting that aggregation was completed. It should be pointed out that aggregation of particles makes the separation of crystalline phases almost impossible.

To avoid the aggregation of particles, the ultrasonic agitation was additionally applied (**Fig. S1** D). Indeed, the sonication inhibited the balls' formation during the mechanical vibration. Moreover, the partial phase separation could be observed for the short vibration duration (till 4 h), as shown in **Fig. 1**. Surprisedly, prolonged vibration caused the mixing of all particles again, probably due to the intense movements of all particles in the cylinder, as already reported [62]. Under the vertical vibration, the particles move from the top to the bottom near the walls of the cylinder and from the bottom to the top in the cylinder center. Interestingly, a decrease in photocatalytic activity with an increase in the vibration duration has been observed **(Fig. 1** C). One could expect that the change in an anatase to rutile ratio could result in an activity change, but the samples sonicated and vibrated for 2, 6 and 8 h are characterized by almost the same composition, and thus other factors should be considered. Accordingly, it has been proposed that sonication-assisted vibration could destroy a crystalline surface of titania (similar to ball milling [71]), resulting in the higher density of deep electron traps (ETs), and thus the lower level of photocatalytic activity.

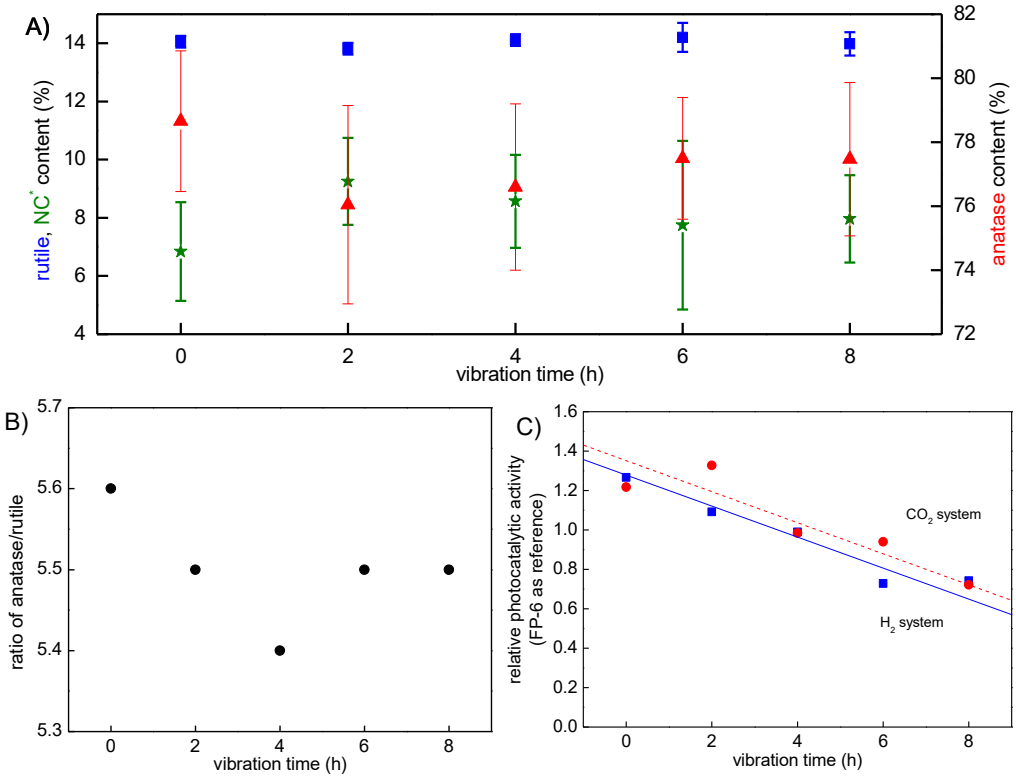

Fig. 1 The characterization and activity of treated P25 for different durations of sonication-assisted vibration: crystalline composition (A), ratio of anatase/rutile (B), and photocatalytic activities (C).

3.2 Phase isolation by chemical dissolution

3.2.1. Characterization of samples

First, P25 sample was homogenized (as reported previously [53]) to use its uniform form (HomoP25). It has been confirmed that the proposed homogenization method is effective, and thus HomoP25 is well homogenized, containing ca. 78% anatase, 14% rutile and 8% non-crystalline phase, as confirmed by XRD analysis (in comparison to nonuniform original P25 sample – OP25) (**Fig. 2**). Then, HomoP25 sample was used for phase isolation (rutile and anatase), and also as the standard (reference) sample for the photocatalytic activity tests.

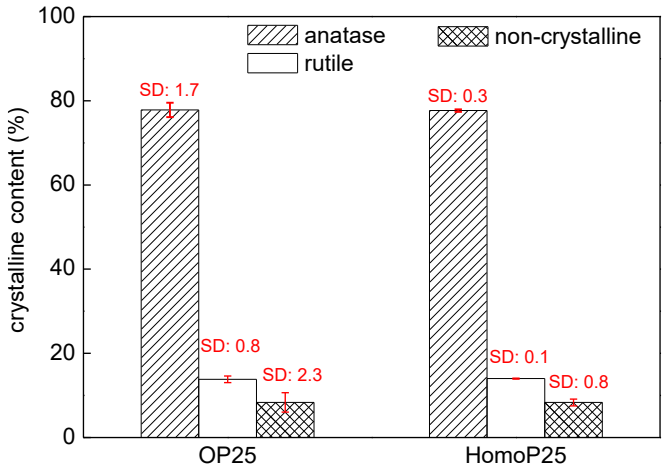

Fig. 2 The crystalline content of OP25 (original P25) and HomoP25 (homogenized P25); SD - standard deviation.

The properties of isolated samples are shown in **Fig. 3**. It is clear that the isolation has resulted in the shift of photoabsorption edge to the shorter wavelengths for iso-ana (**Fig. 3** A) and to the longer wavelengths for iso-rut (**Fig. 3** A), as a result of efficient removal of rutile and anatase, respectively. The stronger absorption of iso-ana at the visible range (400-500 nm) is not surprising since this sample is slightly yellow (inset in **Fig. 3** A). It is thought that some impurities from the isolation process, i.e., inclusion of nitrogen from ammonia or surface peroxy species from hydrogen peroxide, could be responsible for this ~~yellow~~ coloration. The nitrogen-modified titania or titania with adsorbed H_2O_2 (or the complex of [TiO_2-H_2O_2] formed during the isolation process) usually exhibits similar photoabsorption features [72-75]. In contrast, in the case of iso-rut, its photoabsorption is only bathochromically shifted in the comparison to HomoP25, proving the anatase removal since rutile has slightly narrower bandgap than anatase. The slightly stronger photoabsorption at the visible range (400-700 nm) does not result in any change of sample color (the color of iso-rut sample is as white as HomoP25), and thus stronger light scattering on large rutile NPs has initially been considered as the reason of this observation.

The XRD patterns of HomoP25, iso-ana and iso-rut are shown in **Fig. 3** (B). The unnoticeable presence of anatase and rutile in XRD patterns of iso-rut and iso-ana, respectively, confirms that the applied isolation process is efficient to remove anatase and rutile crystallites, respectively. For iso-ana and iso-rut, the width of the most intense anatase and rutile peaks, reflecting the crystallite size, is almost the same as that in HomoP25, confirming that the crystallite sizes do not change during the isolation processes (**Table 1)**, as already reported [63]. The slight decrease in anatase size, i.e., from 25.3 nm to 23.7 nm (and from 39.6 nm to 10.6 nm for rutile), for iso-ana sample suggests the possible co-dissolution of also anatase crystallites together with rutile during titania treatment with the hydrogen peroxide-ammonia mixture. Therefore, the suggested mechanism of dissolution of both crystalline phases but with faster speed for rutile [63] has been proven. For iso-rut sample, the slight increase in crystallite size of rutile (from 39.6 to 42.1 nm) and the disappearance of anatase indicate that the treatment with F could slightly change the surface properties of rutile and preferably dissolve anatase, confirming that anatase is less stable than rutile [76]. Although crystalline phases are separated efficiently, the content of non-crystalline (NC) components has increased in both isolated samples, as shown in **Table 1**. This could result from: i) dissolution of titania crystallites during the isolation process with the subsequent re-formation into amorphous titania particles, and ii) the formation of NC phase during isolation process from HF, NH_3, H_2O_2, amorphous titania and/or compounds formed during titania dissolution.

In order to remove the possible impurities, originated from the isolation process (such as N and H_2O_2 in iso-ana ~~sample~~ and F in iso-rut ~~sample~~), the post-treatment annealing has been applied. The DRS data for the annealed samples are shown in **Fig. 3** C and D. Indeed, the annealing causes the disappearance of vis absorption for iso-ana sample, indicating an efficient removal of contaminants. It should be pointed out that the crystalline content of anatase does not change significantly by the post-treatment (84-90%). On the other hand, the content of NC part and the crystallite sizes for both anatase and residual rutile are quite different in the samples annealed at different conditions. It is known that thermal treatment results in both the acceleration of the crystal growth and the phase conversion, i.e., from amorphous phase via anatase to rutile. However, a decrease in rutile size could not be explained by the crystal growth mechanism. Therefore, it is expected that the formation of new rutile NPs from amorphous phase and/or fine anatase NPs could be responsible for the formation of fine rutile NPs. Anyway, it is thought that rutile as well as amorphous phase (7-17%) might be neglected in the overall photocatalytic activity since rutile content is too low (1-4%) [64] and amorphous phase is considered as inactive under UV irradiation [20,77].

Interestingly, quite different behavior is noticed for the annealed iso-rut samples, as shown in **Fig. 3** D. The shapes of DRS spectra, especially for the samples annealed at 120 ºC and 200 ºC, differ significantly from that of iso-rut, with significant photoabsorption in the vis range, as clearly observed even by the change in sample color, i.e., from white to light brown (inset in **Fig. 4**). It is proposed that

a shoulder at 400-800 nm could originate from either trivalent titanium species or titania modified with adsorbed hydrofluoric (HF) acid. Moreover, the post-treatment annealing has caused the change in the crystalline composition, as NC content has increased significantly, i.e., from 11 to 16, 21, 23 and 28% for samples annealed at 120, 200, 300 and 500 °C, respectively. It is proposed that HF etching has resulted in the dissolution of titania crystals and the simultaneous formation of F-modified titania of amorphous nature. Moreover, a high amount of NC phase and a decrease in rutile content for the samples annealed at higher temperatures indicate that annealing accelerates the reaction between rutile and HF adsorbed on its surface, and thus new amorphous compounds containing titanium, fluorine, hydrogen and oxygen could be formed. It should be pointed out that much different behavior is observed for the annealed iso-ana samples, where annealing has caused a disappearance of vis absorption for all materials, as well as a decrease in the NC content for iso-ana-120 and iso-ana-300 samples. However, an increase in annealing temperature to 500 ºC has caused an increase in the NC content, which could be caused by a similar mechanism to already proposed for annealed rutile, i.e., chemical compounds, used for anatase isolation (NH_3, H_2O_2), adsorbed on the titania surface, could react with crystalline anatase at high temperature, causing its dissolution and the formation of new amorphous compounds consisting of titanium, oxygen, nitrogen and hydrogen.

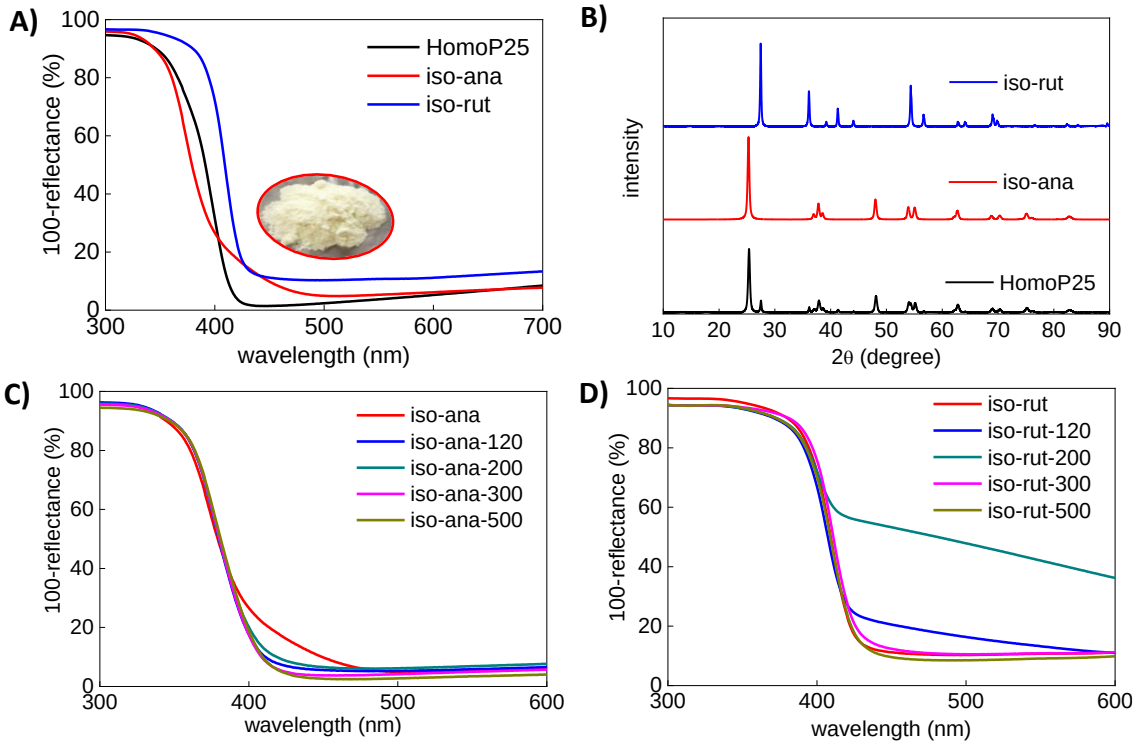

Fig. 3 The photoabsorption properties (A) and XRD patterns (B) of isolated samples: HomoP25, iso-ana (with photo) and iso-rut, and photoabsorption properties of annealed isolated samples: (C) anatase samples and (D) rutile samples.

To remove hydrofluoric acid from the surface of isolated rutile (iso-rut) and to avoid the formation of F-modified titania (during annealing), iso-rut has been washed with aqueous solution of NaOH, and

then annealed. Indeed, the removal of HF by NaOH washing is very efficient, and the surface content of fluorine, measured by XPS, has been reduced from 9% to less than 1% (**Fig. S4 and Fig. S5**). Moreover, the high vis photoabsorption of isolated rutile sample has disappeared, as shown in **Fig. 4**. The crystalline compositions of washed samples annealed at different temperatures are shown in **Table 2**. The content of NC phase in these samples is much lower than that in unwashed ones, proving the removal of formed impurities from the surface of the iso-rut. Interestingly, only non-annealed sample (iso-rut-NaOH) possesses higher NC content than that in unwashed sample (iso-rut), suggesting that not only acidic, but also alkali treatment might cause the dissolution of crystalline phases and the formation of amorphous compounds. Accordingly, it has been concluded that iso-ana-200 and iso-rut-NaOH-200 are the most adequate samples to be used (as the purest) for further detailed studies.

Table 1. The phase content and crystallites size of isolated sample and HomoP25

sample	calcination temp. (°C)	phase content (%)			crystallite size (nm)	
		anatase	Rutile	NC	anatase	rutile
HomoP25	-	78	14	8	25.3	39.6
iso-ana	-	86	1	13	23.7	10.6
iso-ana-120	120	84	4	12	25.9	6.8
iso-ana-200	200	86	1	13	28.9	3.9
iso-ana-300	300	90	3	7	31.6	7.8
iso-ana-500	500	83	0	17	39.1	-
iso-rut	-	0	89	11	-	42.1
iso-rut-120	120	0	84	16	-	44.6
iso-rut-200	200	0	76	21	-	49.6
iso-rut-300	300	1	76	23	17.4	55.1
iso-rut-500	500	1	72	28	1.3	70.9

NC: non-crystalline phase

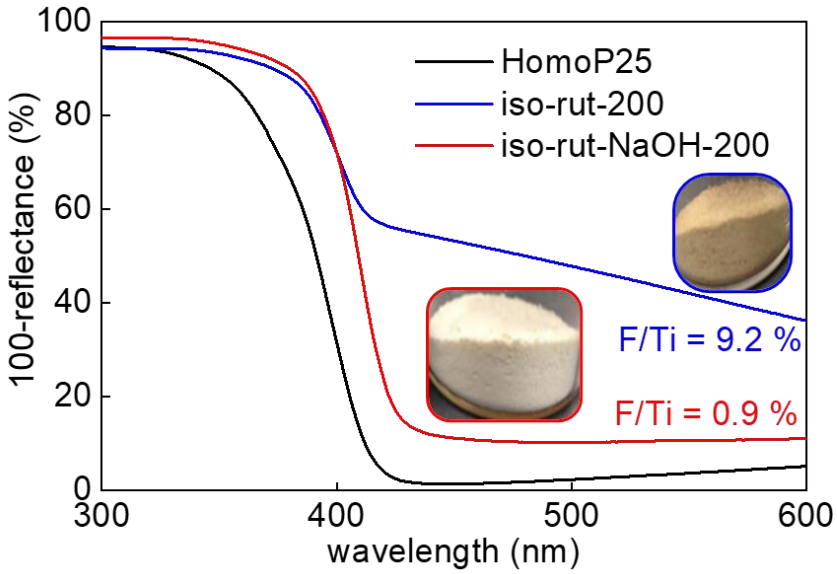

Fig. 4 Photoabsorption of iso-rut-200, iso-rut-NaOH-200 and HomoP25.

334 **Table 2**. Crystalline composition of washed samples

Sample	calcination temp. (°C)	phase content (%)			crystallite size (nm)	
		anatase	rutile	NC	anatase	Rutile
iso-rut-NaOH	-	0	84	16	-	47.3
iso-rut-NaOH-120	120	0	89	11	-	47.1
iso-rut-NaOH-200	200	1	97	2	10.4	46.6
iso-rut-NaOH-300	300	0	80	19	-	47.3
iso-rut-NaOH-500	500	0	84	16	-	53.1

335 NC: non-crystalline phase

336

337 Next, the morphology of samples has also been investigated, and exemplary STEM images are
338 shown in **Fig. 5**. The presence of titania particles of different sizes (from 15 to 150 nm) is observed in
339 HomoP25 sample. The comparison with isolated samples allows to conclude that particles of rutile
340 and anatase are larger and smaller, respectively. The particle size of rutile varies from 20 to 150 nm,
341 whereas that in anatase from 15 to 60 nm. The existence of rutile and anatase in the form of larger and
342 smaller NPs, respectively, is not surprising since usually rutile forms larger NPs (Rutile is the most
343 stable polymorph of titania, and thus particles of metastable anatase coalesce and transform to rutile
344 [78].). It should be mentioned that average sizes of isolated phases, estimated from STEM images, are
345 only slightly smaller than crystallite sizes, i.e., for anatase of ca. 23.3 nm (STEM) and 28.9 nm (XRD)
346 and for rutile of ca. 40.2 nm (STEM) and 46.6 nm (XRD), indicating that many particles are single
347 crystals. Moreover, the average size of NPs in HomoP25 (27.5 nm) is practically same as weighted
348 average size of anatase and rutile crystallites (27.4 nm). Therefore, it might be concluded that
349 multiphase particles (anatase-rutile, anatase-amorphous, rutile-amorphous) are not the main
350 component of P25, in contrast to some previous reports, suggesting that anatase/rutile composites are
351 mostly responsible for the high activity of P25, e.g., anatase with rutile overlayer [46]. However, it is
352 also possible that some multiphase particles exist in P25, and that the charge transfer between anatase
353 and rutile is still possible, even if the contact between them is not perfect. Additionally, it must be
354 mentioned that in the contrast to HomoP25, isolated samples contain also large aggregates, resulting
355 from thermally initiated particles' sintering. Therefore, even if the composition and crystallite sizes of
356 isolated samples are almost the same as expected (after phase separation from P25), the physical
357 properties have been slightly changed during isolation, e.g., NPs' aggregation.

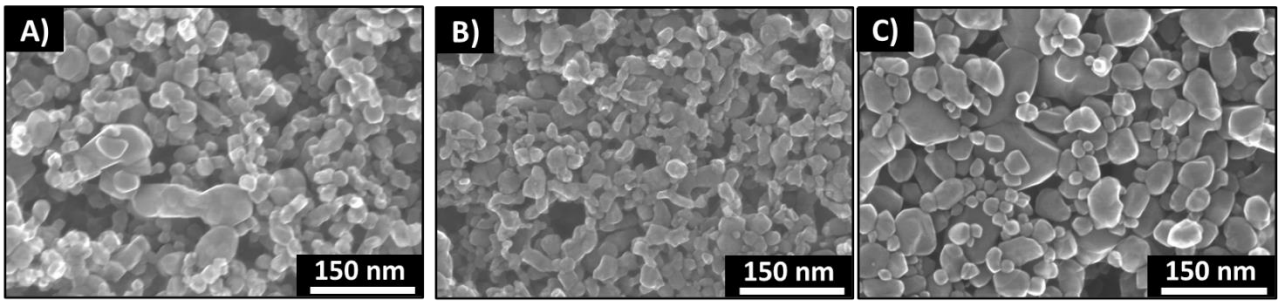

D) SSA and particle size of samples

sample	SSA (BET)	Particle size/nm (PS*)	Particle size/nm (STEM)	
	/m^{2}g^{-1}		average	mean
HomoP25	52	28.8	27.5	22.5
ANA	61	24.6	23.3	19.5
RUT	28	53.6	40.2	32.4

PS*: particle size was calculated by SSA with the relationship: 1500=SSA* particle size

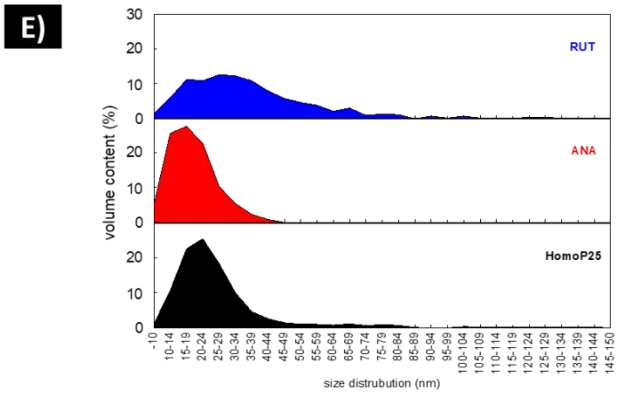

Fig. 5 STEM images (A-C) and estimated data for particle size (D-E): A) for HomoP25, B) iso-ana-200, and C) iso-rut-NaOH-200; iso-ana-200 (ANA), iso-rut-NaOH-200 (RUT).

3.2.2. Photocatalytic activity

The photocatalytic activities of isolated samples and HomoP25 were checked for oxidative decomposition of acetic acid (CO_2 system) and dehydrogenation of methanol (H_2 system). The summarized results in respect to activity of HomoP25 (normalize activity when 1.0 is taken for HomoP25) are shown in **Fig. 6**. Isolated samples without any purification (iso-rut and iso-ana) have shown low activity in the H_2 system, but iso-ana exhibits higher activity in the CO_2 system than HomoP25, as already reported [20]. The higher activity of iso-ana than that of HomoP25 and iso-rut could be caused by: i) slightly more negative position of CB of anatase than that of rutile [65,66,79-81], or in contradiction ii) more positive position of VB of anatase, as recently suggested by Buchalska et al. [82], and thus stronger oxidation ability by positive holes. The purification by annealing does not change the overall activities drastically in CO_2 system, i.e., similarly to no-treated samples, where anatase is the most active phase. Interestingly, iso-rut-200 with the strongest vis-absorption shows also the highest activity among rutile samples, which could be caused by titania modification with fluorine. Some recent reports have indicated that such modification might enhance the photocatalytic activity [83,84]. Moreover, the purification of isolated rutile by washing with NaOH has resulted in a slight decrease in the activity in CO_2 system, which could be caused by the presence of sodium. It is well known that sodium hinders the photocatalytic activity of titania, being a recombination center (the largest problem of titania coatings applied on the sodium glass) [32,85].

Interestingly, much higher activity of HomoP25 in H_2 system than that of single crystalline phases could confirm the "synergy" between two phases (the activity of P25 is higher than the sum of activities of iso-ana and iso-rut), e.g., via IPCT ~~(inter particle charge transfer)~~. However, it should be remembered that these isolated samples are not pure. Interestingly, the activity of two purified rutile samples (iso-rut-NaOH-200 and iso-rut-NaOH-300) are higher than that by HomoP25. It seems that sodium does not influence the activity since co-deposited platinum works also as an inhibitor of charge carriers' recombination. Accordingly, it has been confirmed that the high activity of P25 could be explained by high intrinsic properties of its components, i.e., anatase and rutile, in oxidation and reduction reactions, respectively. Similar findings have recently been found by Macyk group, i.e., rutile with more negative CB level, resulting in more efficient reduction pathway, and anatase as a stronger oxidant with efficient $HO^{\bullet}$ generation [82].

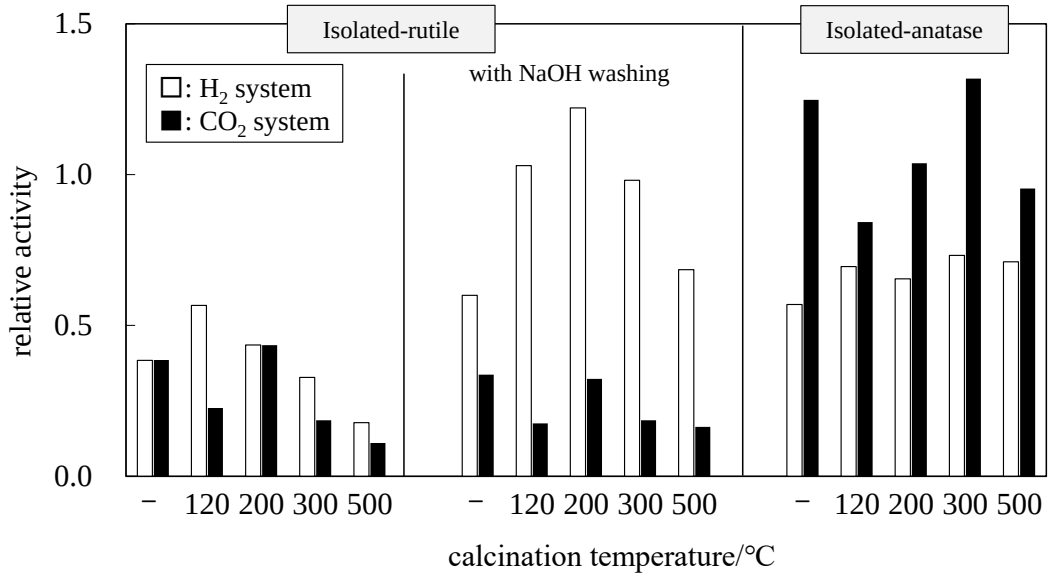

Fig. 6 The photocatalytic activity of isolated samples in two reaction systems (photocatalytic activity of HomoP25 = 1); "-": without annealing.

To understand the difference between anatase and rutile in P25, i.e., charge carriers' migration, electron lifetime and electron traps (ETs) distribution, TRMC and RDB-PAS investigations have been carried out for three samples: HomoP25, iso-ana-200 and iso-rut-NaOH-200, and obtained data are shown in **Figs. 7** and **8**. After UV-excitation, TRMC signal appears, as shown in **Fig. 7** A. Most intensive TRMC signal (I_{max}) for pure isolated anatase than for HomoP25 and the less intensive for pure isolated rutile might confirm that anatase is responsible for high photocatalytic activity, as usually reported [86-88], i.e., the high content of generated charge carriers. The similar decay (speed of charge carriers' recombination, **Fig. 7** B) for iso-ana-200 and HomoP25 confirms that the high activity of P25 is caused by the anatase presence. The faster decay for rutile sample as well as the lowest I_{max} indicate that photogenerated electrons are trapped fast at the recombination centers. It is thought that even if

co-deposited platinum hinders the charge carriers' recombination, its presence does not explain the highest activity of rutile-based samples for methanol dehydrogenation since not only the fastest signal decay but also much less intensive TRMC signal (and thus lower number of photogenerated electrons) have been observed in rutile. Therefore, high activity of rutile in H_2 system should be caused by more negative CB position, and thus its higher reduction ability than that in anatase and HomoP25 (with majority of anatase).

TRMC data confirm that usually anatase is more active than rutile (as also shown here for CO_2 system) due to longer lifetime (slower decay) and a larger number (more intensive signal) of photogenerated charge carriers. Accordingly, it is proposed that the higher activity of anatase than rutile is caused by the intrinsic properties of both phases, i.e., the larger content of deeper electron traps (ETs) in rutile than that in anatase, resulting in fast charge carriers' recombination. Indeed, RDB-PAS experiments have confirmed this hypothesis, showing the larger content of shallow ETs in isolated anatase sample (inside or just below bottom of CB) and the larger content of deeper ETs (inside bandgap) in isolated rutile samples, as shown in **Fig. 8**.

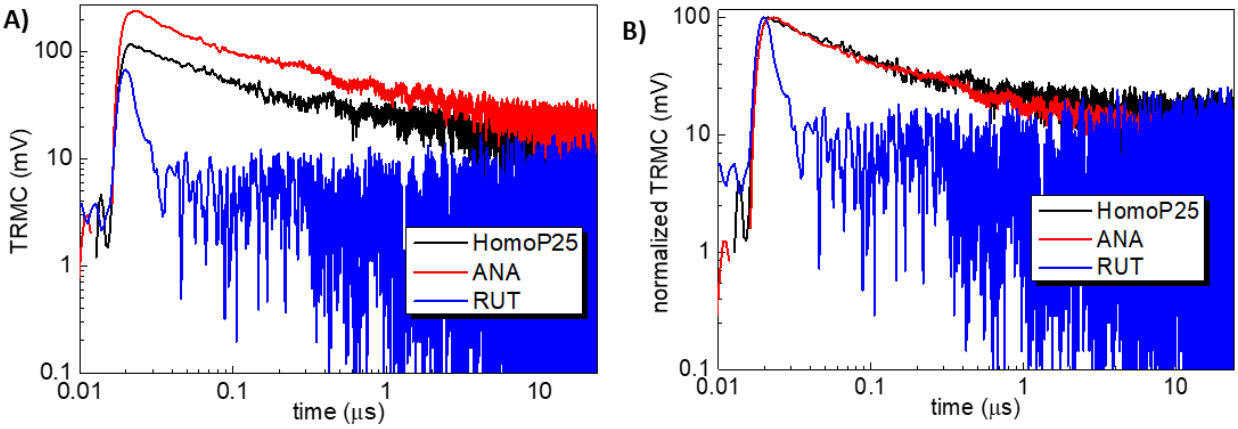

Fig. 7 The TRMC results of HomoP25, iso-ana-200 (ANA) and iso-rut-NaOH-200 (RUT): A) original and B) normalized data.

Based on TRMC and RDB-PAS data, it is difficult to explain the surprisingly high activity of rutile ~~sample~~ in H_2 system, i.e., by mobility and lifetime of electrons, as well as distribution of ETs. There are two possible explanations: i) narrower bandgap, and thus ability to absorb more photons, and ii) more negative CB of rutile than that of anatase, as suggest by Scanlon et al. [89] and Buchalska et al. [82], and discussed above. Moreover, it should be stressed that in H_2 system, Pt deposits are used as a co-catalyst (Titania is practically inactive in this system due to high activation overpotential for hydrogen evolution.). Therefore, Pt NPs works as active sites for hydrogen evolution, but also as an electron pool (as a result of higher work function than electron affinity of titania), hindering the recombination between electrons and holes, as firstly reported by A. J. Bard in 1970s [90,91]. Therefore, also properties of platinum deposits could influence the overall activity, as already discussed in our

previous study [53].

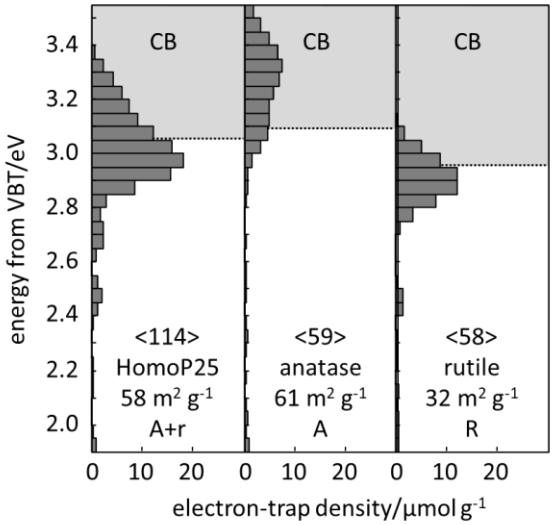

Fig. 8 The RDB-PAS results of HomoP25, iso-ana-200 (anatase) and iso-rut-NaOH-200 (rutile); Data shown in brackets indicate the total density of ETs in the unit of mmol g^{-1}. Specific surface area in the unit of m^2 g^{-1} is shown in the third row. Abbreviations ''A'' and ''R'' in the bottom row is for majority component, i.e., anatase and rutile, respectively, and ''a'' and ''r'' are anatase and rutile as minor component, respectively.

Since some of the isolated samples show vis absorption, the vis activity has also been measured, and obtained data are presented in **Fig. 9**. Indeed, the samples with vis absorption ability exhibit also vis activity. In the case of the anatase samples, iso-ana with yellow color shows the highest response, and thus confirming that titania modification with either nitrogen [92-95] or hydrogen peroxide [96-100] might cause the vis response. In the case of rutile samples, simple isolation followed by annealing results in the coloration of two samples (iso-rut-120 and iso-rut-200) with also the highest vis activity. Interestingly, washing with NaOH causes a significant increase in vis activity, especially for the sample annealed at 200 °C (iso-rut-NaOH-200). Therefore, it might be concluded that sodium-based modifiers, which are not recommended under UV irradiation (working as charge carriers' recombination centers), might initiate vis action of titania. However, it is also possible that co-present fluorine is also involved as clearly seen by the comparison between iso -rut-NaOH-200 and iso -rut-200-NaOH-200. Both samples were washed with NaOH and then annealed at 200 °C, but the most active sample (iso -rut-200-NaOH-200) was also annealed just after isolation (similar to the most active non-washed sample – iso-rut-200**)**, which might indicate that the present fluorine on the rutile surface could be partially doped/adsorbed under the thermal treatment. Then, washing with NaOH might cause the co-modification (F/Na) of titania. Interestingly, NaF is commonly used for the preparation of F-modified/doped titania samples, and NaOH is applied for the sample washing [101]. Additionally, the possibility of an existence of additional energy levels inside the bandgap of titania, due to doping and self-doping (the formation of defective titania because of thermal treatment [102]) should also be

considered. The further studies on these aspects are now in progress, including the detailed characterization of all samples (RDB-PAS and XPS), as well as the preparation of other vis responsive materials.

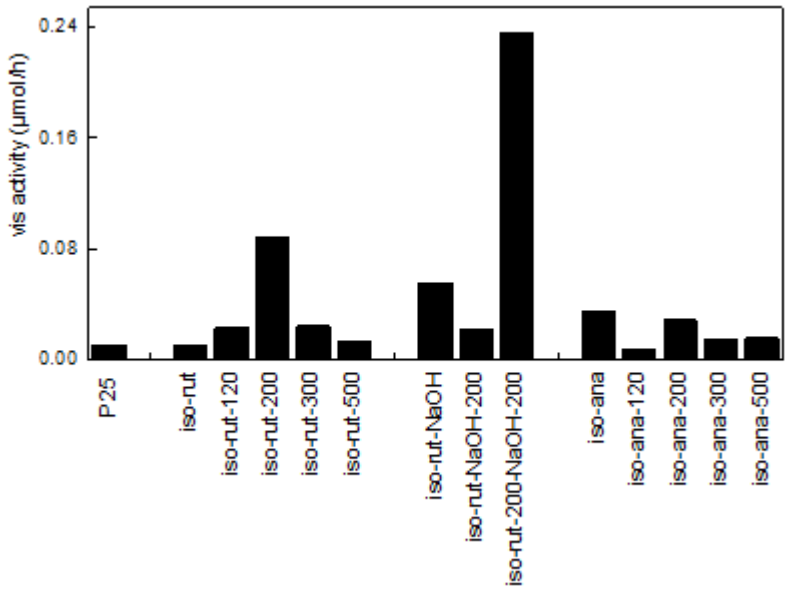

Fig. 9 The vis activity of samples for 2-propanol oxidation ($\lambda > 450$ nm).

Summary and conclusions

Two isolation methods have been used for the separation of the active components in P25, i.e., (i) physical by vibration and sonication-assisted vibration, and (ii) chemical by dissolution. Unfortunately, though physical method is more recommended since it does not result in any change in the chemical composition of sample (impurity), it is not efficient for the separation of anatase, rutile and amorphous phase. Interestingly, it has been found that the sonicated-vibrated samples have lost some photocatalytic activity, and thus it is suggested that the thermal energy has caused a slight destruction of the particles' surface (possible formation of deep ETs), similar to the ball-milled samples [71].

In contrast, the chemical methods, used for the isolation of anatase and rutile from homogenized P25 (a uniform sample) show to be effective. However, at the same, chemical compounds used for the samples' etching are adsorbed on the titania surface as impurities. Accordingly, their removal must be applied. It has been found that: (i) the thermal treatment of isolated anatase, and (ii) the washing with NaOH followed by thermal treatment of isolated rutile, are quite efficient in the removal of these impurities. The purified anatase and the purified rutile exhibit high photocatalytic activity in oxidative decomposition of acetic acid and dehydrogenation of methanol, respectively, reaching higher levels of activity than those by homogenized P25 (HomoP25), and thus confirming that the origin of the high activity of P25 is due to the intrinsic activities of both phases rather than the charge carriers' migration between them. The TRMC and RDB-PAS data have confirmed the higher mobility, longer lifetime of

charge carriers' and shallower ETs for anatase than for rutile, and thus its commonly better activity (especially in oxidative reactions). Interestingly, the isolated samples also exhibit some vis activity due to the surface modifications with impurities, e.g., N, H_2O_2, F and Na. Therefore, it might be concluded that sodium, despite detrimental effect on UV-titania activity, might activate titania towards vis response.

Although, the chemical isolation followed by the purification has resulted in an efficient separation of almost pure polymorphs with similar properties as those in original P25, the isolated particles are not exactly same as those in P25 since the physical properties have slightly been changed during the isolation, e.g., NPs' aggregation. Moreover, it is impossible to get an original amorphous titania by the chemical dissolution methods, as probably the amorphous phase dissolves first. Accordingly, other "non-invasive" methods (e.g., physical separation) are highly wanted to confirm the properties, and thus activities of rutile, anatase and amorphous titania in famous P25 photocatalyst.

References

1. M. R. Hoffmann; S. T. Martin; W. Y. Choi; D. W. Bahnemann. Environmental applications of semiconductor photocatalysis. *Chem. Rev.* **1995**, *95*, 69-96; doi:10.1021/cr00033a004
2. A. Fujishima; K. Honda. Electrochemical photolysis of water at a semiconductor electrode. *Nature* **1972**, *238*, 37-38.
3. S. Malato; J. Blanco; C. Richter; D. Curco; J. Gimenez. Low-concentrating CPC collectors for photocatalytic water detoxification: comparison with a medium concentrating solar collector. *Wat. Sci. Technol.* **1997**, *35*, 157-164.
4. C. Minero; E. Pelizzetti; S. Malato; J. Blanco. Large solar plant photocatalytic water decontamination: Degradation of pentachlorophenol *Chemosphere* **1993**, *26*, 2103-2119.
5. B. Ohtani; S.-i. Nishimoto. Effect of surface adsorption of aliphatic alcohols and silver ion on the photocatalytic activity of TiO_2 suspended in aqueous solutions. *J. Phys. Chem. B* **1993**, *97*, 920-926.
6. A. Markowska-Szczupak; P. Rokicka; K. L. Wang; M. Endo; A. W. Morawski; E. Kowalska. Photocatalytic Water Disinfection under Solar Irradiation by D-Glucose-Modified Titania. *Catalysts* **2018**, *8*, doi:10.3390/Catal8080316.
7. B. Zielinska; J. Grzechulska; B. Grzmil; A. W. Morawski. Photocatalytic degradation of Reactive Black 5 - A comparison between TiO_2-Tytanpol A11 and TiO_2-Degussa P25 photocatalysts. *Appl. Catal. B-Environ.* **2001**, *35*, L1-L7, doi:10.1016/S0926-3373(01)00230-2.
8. B. O'Regan; F. Lenzmann; R. Muis; J. Wienke. A solid-state dye-sensitized solar cell fabricated with pressure-treated P25-TiO_2 and CuSCN: Analysis of pore filling and IV characteristics. *Chem. Mat.* **2002**, *14*, 5023-5029, doi:10.1021/cm020572d.
9. D. C. Hurum; A. G. Agrios; K. A. Gray; T. Rajh; M. C. Thurnauer. Explaining the enhanced photocatalytic activity of Degussa P25 mixed-phase TiO_2 using EPR. *J. Phys. Chem. B* **2003**, *107*, 4545-4549, doi:10.1021/jp0273934.

10. J. Grzechulska; A. W. Morawski. Photocatalytic labyrinth flow reactor with immobilized P25 TiO2 bed for removal of phenol from water. *Appl. Catal. B: Environ.* **2003**, *46*, 415-419, doi:10.1016/s0926-3373(03)00265-0.
11. K. Demeestere; J. Dewulf; H. Van Langenhove; B. Sercu. Gas-solid adsorption of selected volatile organic compounds on titanium dioxide Degussa P25. *Chem. Eng. Sci.* **2003**, *58*, 2255-2267, doi:10.1016/S0009-2509(03)00087-3.
12. D. C. Hurum; K. A. Gray; T. Rajh; M. C. Thurnauer. Photoinitiated reactions of 2,4,6 TCP on Degussa P25 formulation TiO_2: Wavelength-sensitive decomposition. *J. Phys. Chem. B* **2004**, *108*, 16483-16487, doi:10.1021/jp047097m.
13. D. C. Hurum; K. A. Gray; T. Rajh; M. C. Thurnauer. Recombination pathways in the Degussa P25 formulation of TiO_2: Surface versus lattice mechanisms. *J. Phys. Chem. B* **2005**, *109*, 977-980, doi:10.1021/Jp015395d.
14. W. Y. Teoh; L. Madler; D. Beydoun; S. E. Pratsinis; R. Amal. Direct (one-step) synthesis of TiO_2 and Pt/TiO_2 nanoparticles for photocatalytic mineralisation of sucrose. *Chem. Eng. Sci.* **2005**, *60*, 5852-5861, doi:10.1016/j.ces.2005.05.037.
15. J. Kirchnerova; M. L. H. Cohen; C. Guy; D. Klvana. Photocatalytic oxidation of n-butanol under fluorescent visible light lamp over commercial TiO_2 (Hombicat UV100 and Degussa P25). *Appl. Catal. A-Gen.* **2005**, *282*, 321-332, doi:10.1016/j.apcata.2004.12.045.
16. J. G. Yu; H. G. Yu; B. Cheng; M. H. Zhou; X. J. Zhao. Enhanced photocatalytic activity of TiO_2 powder (P25) by hydrothermal treatment. *J. Mol. Catal. A-Chem.* **2006**, *253*, 112-118, doi:10.1016/j.molcata.2006.03.021.
17. T. C. Long; N. Saleh; R. D. Tilton; G. V. Lowry; B. Veronesi. Titanium dioxide (P25) produces reactive oxygen species in immortalized brain microglia (BV2): Implications for nanoparticle neurotoxicity. *Environ. Sci. Technol.* **2006**, *40*, 4346-4352, doi:10.1021/es060589n.
18. M. Janus; A. W. Morawski. New method of improving photocatalytic activity of commercial Degussa P25 for azo dyes, decomposition. *Appl. Catal. B-Environ.* **2007**, *75*, 118-123, doi:10.1016/j.apeatb.2007.04.003.
19. A. Mills; S. K. Lee. A web-based overview of semiconductor photochemistry-based current commercial applications. *J. Photochem. Photobiol. A* **2002**, *152*, 233-247, doi:Pii S1010-6030(02)00243-5, doi 10.1016/S1010-6030(02)00243-5.
20. B. Ohtani; O. O. Prieto-Mahaney; D. Li; R. Abe. What Is Degussa (Evonik) P25 Crystalline Composition Analysis, Reconstruction from Isolated Pure Particles and Photocatalytic Activity Test. *J. Photochem. Photobiol. A* **2010**, *216*, 179.
21. B. Neppolian. Solar/UV-induced photocatalytic degradation of three commercial textile dyes. *J. Hazard. Mater.* **2002**, *89*, 303-317, doi:10.1016/s0304-3894(01)00329-6.
22. A. Mills; S. Morris. Photomineralization of 4-Chlorophenol Sensitized by Titanium-Dioxide - a Study of the Initial Kinetics of Carbon-Dioxide Photogeneration. *J. Photochem. Photobiol. A* **1993**, *71*, 75-83, doi:10.1016/1010-6030(93)87012-C.
23. S. Mozia; M. Tomaszewska; A. W. Morawski. A new photocatalytic membrane reactor (PMR) for removal of azo-dye Acid Red 18 from water. *Appl. Catal. B: Environ.* **2005**, *59*, 131-137, doi:10.1016/j.apcatb.2005.01.011.

24. B. Toepfer; A. Gora; G. Li Puma. Photocatalytic oxidation of multicomponent solutions of herbicides: Reaction kinetics analysis with explicit photon absorption effects. *Appl. Catal. B-Environ.* **2006**, *68*, 171-180, doi:10.1016/j.apcatb.2006.06.020.
25. M. A. Ferguson; J. G. Hering. TiO_2-photocatalyzed As(III) oxidation in a fixed-bed, flow-through reactor. *Environ. Sci. Technol.* **2006**, *40*, 4261-4267, doi:10.1021/es0524853.
26. Z. X. Yao; M. Q. Wang; S. H. Sun; R. B. Jia; H. Li. High Performance Photocatalysts Based on N-doped Graphene-P25 for Photocatalytic Reduction of Carbon Tetrachloride. *J. Inorg. Organomet. P* **2014**, *24*, 315-320, doi:10.1007/s10904-013-9960-4.
27. Y. C. Jiao; H. L. Jiang; F. Chen. RuO_2/TiO_2/Pt Ternary Photocatalysts with Epitaxial Heterojunction and Their Application in CO Oxidation. *ACS Catal.* **2014**, *4*, 2249-2257, doi:10.1021/cs5001174.
28. F. Thevenet; C. Guillard; A. Rousseau. Acetylene photocatalytic oxidation using continuous flow reactor: Gas phase and adsorbed phase investigation, assessment of the photocatalyst deactivation. *Chem. Eng. J.* **2014**, *244*, 50-58, doi:10.1016/j.cej.2014.01.038.
29. H. Sakai; Y. Kubota; K. Yamaguchi; H. Fukuoka; K. Inumaru. Photocatalytic decomposition of 2-propanol and acetone in air by nanocomposites of pre-formed TiO_2 particles and mesoporous silica. *J. Porous Mater.* **2012**, *20*, 693-699, doi:10.1007/s10934-012-9643-5.
30. F.-L. Toma; G. Bertrand; S. O. Chwa; C. Meunier; D. Klein; C. Coddet. Comparative study on the photocatalytic decomposition of nitrogen oxides using TiO_2 coatings prepared by conventional plasma spraying and suspension plasma spraying. *Surf. Coat. Technol.* **2006**, *200*, 5855-5862, doi:10.1016/j.surfcoat.2005.08.148.
31. N. Nishikawa; S. Kaneco; H. Katsumata; T. Suzuki; K. Ohta; E. Yamazaki; K. Masuyama; T. Hashimoto; K. Kamiya. Photocatalytic degradation of allergens in water with titanium dioxide. *Fresenius Environ. Bull.* **2007**, *16*, 310-314.
32. A. Markowska-Szczupak; K. L. Wang; P. Rokicka; M. Endo; Z. S. Wei; B. Ohtani; A. W. Morawski; E. Kowalska. The effect of anatase and rutile crystallites isolated from titania P25 photocatalyst on growth of selected mould fungi. *J. Photochem. Photobiol. B* **2015**, *151*, 54-62, doi:10.1016/j.jphotobiol.2015.07.002.
33. V. Krishna; S. Pumprueg; S. H. Lee; J. Zhao; W. Sigmund; B. Koopman; B. M. Moudgil. Photocatalytic disinfection with titanium dioxide coated multi-wall carbon nanotubes. *Process Saf. Environ.* **2005**, *83*, 393-397, doi:10.1205/psep.04387.
34. A. K. Benabbou; Z. Derriche; C. Felix; P. Lejeune; C. Guillard. Photocatalytic inactivation of Escherischia coli - Effect of concentration of TiO_2 and microorganism, nature, and intensity of UV irradiation. *Appl. Catal. B-Environ.* **2007**, *76*, 257-263, doi:10.1016/j.apcatb.2007.05.026.
35. A. Bozzi; T. Yuranova; I. Guasaquillo; D. Laub; J. Kiwi. Self-cleaning of modified cotton textiles by TiO2 at low temperatures under daylight irradiation. *J. Photochem. Photobiol. A* **2005**, *174*, 156-164, doi:10.1016/j.jphotochem.2005.03.019.
36. M. Smits; C. k. Chan; T. Tytgat; B. Craeye; N. Costarramone; S. Lacombe; S. Lenaerts. Photocatalytic degradation of soot deposition: Self-cleaning effect on titanium dioxide coated cementitious materials. *Chem. Eng. J.* **2013**, *222*, 411-418,

606 doi:10.1016/j.cej.2013.02.089.
607 37. N. Vero; S. Hribernik; P. Andreozzi; M. Sfiligoj-Smole. Homogeneous self-cleaning
608 coatings on cellulose materials derived from TIP/TiO_2 P25. *Fibers Polym.* **2009**, *10*, 716-
609 723, doi:10.1007/s12221-010-0716-2.
610 38. M. Antoniadou; P. Lianos. Production of electricity by photoelectrochemical oxidation of
611 ethanol in a PhotoFuelCell. *Appl. Catal. B-Environ.* **2010**, *99*, 307-313,
612 doi:10.1016/j.apcatb.2010.06.037.
613 39. K. Suttiponparnit; J. K. Jiang; M. Sahu; S. Suvachittanont; T. Charinpanitkul; P. Biswas. Role
614 of Surface Area, Primary Particle Size, and Crystal Phase on Titanium Dioxide
615 Nanoparticle Dispersion Properties. *Nanoscale Res. Lett.* **2011**, *6*, 8, doi:10.1007/s11671-
616 010-9772-1.
617 40. T. Froschl; U. Hormann; P. Kubiak; G. Kucerova; M. Pfanzelt; C. K. Weiss; R. J. Behm; N.
618 Husing; U. Kaiser; K. Landfester; et al. High surface area crystalline titanium dioxide:
619 potential and limits in electrochemical energy storage and catalysis. *Chem. Soc. Rev.*
620 **2012**, *41*, 5313-5360, doi:10.1039/c2cs35013k.
621 41. L. Andronic; D. Andrasi; A. Enesca; M. Visa; A. Duta. The influence of titanium dioxide
622 phase composition on dyes photocatalysis. *J. Sol.-Gel Sci. Techn.* **2011**, *58*, 201-208,
623 doi:10.1007/s10971-010-2378-3.
624 42. P. Apopei; C. Catrinescu; C. Teodosiu; S. Royer. Mixed-phase TiO_2 photocatalysts:
625 Crystalline phase isolation and reconstruction, characterization and photocatalytic
626 activity in the oxidation of 4-chlorophenol from aqueous effluents. *Appl. Catal. B-Environ.*
627 **2014**, *160*, 374-382, doi:10.1016/j.apcatb.2014.05.030.
628 43. K. V. Baiju; A. Zachariah; S. Shukla; S. Biju; M. L. P. Reddy; K. G. K. Warrier. Correlating
629 Photoluminescence and Photocatalytic Activity of Mixed-phase Nanocrystalline Titania.
630 *Catal. Lett.* **2009**, *130*, 130-136, doi:10.1007/s10562-008-9798-5.
631 44. M. Boehme; W. Ensinger. Mixed Phase Anatase/rutile Titanium Dioxide Nanotubes for
632 Enhanced Photocatalytic Degradation of Methylene-blue. *Nano-Micro Lett.* **2011**, *3*,
633 236-241, doi:10.1007/Bf03353678.
634 45. Z. B. Zhang; C. C. Wang; R. Zakaria; J. Y. Ying. Role of particle size in nanocrystalline TiO_2-
635 based photocatalysts. *J. Phys. Chem. B* **1998**, *102*, 10871-10878, doi:10.1021/jp982948+.
636 46. R. I. Bickley; T. Gonzalezcarreno; J. S. Lees; L. Palmisano; R. J. D. Tilley. A Structural
637 Investigation of Titanium-Dioxide Photocatalysts. *J. Solid State Chem.* **1991**, *92*, 178-190,
638 doi:10.1016/0022-4596(91)90255-G.
639 47. X. Z. Jiang; M. Manawan; T. Feng; R. F. Qian; T. Zhao; G. D. Zhou; F. T. Kong; Q. Wang; S.
640 Y. Dai; J. H. Pan. Anatase and rutile in evonik aeroxide P25: Heterojunctioned or individual
641 nanoparticles? *Catal. Today* **2018**, *300*, 12-17, doi:10.1016/j.cattod.2017.06.010.
642 48. R. Su; R. Bechstein; L. Sø; R. T. Vang; M. Sillassen; B. Esbjörnsson; A. Palmqvist; F.
643 Besenbacher. How the Anatase-to-Rutile Ratio Influences the Photoreactivity of TiO_2. *J.*
644 *Phys. Chem. C* **2011**, *115*, 24287-24292, doi:10.1021/jp2086768.
645 49. Z. Xiong; H. Wu; L. Zhang; Y. Gu; X. S. Zhao. Synthesis of TiO_2 with controllable ratio of
646 anatase to rutile. *J. Mater. Chem. A* **2014**, *2*, doi:10.1039/c4ta01144a.
647 50. A. Li; Z. Wang; H. Yin; S. Wang; P. Yan; B. Huang; X. Wang; R. Li; X. Zong; H. Han; et al.

Understanding the anatase–rutile phase junction in charge separation and transfer in a TiO_2 electrode for photoelectrochemical water splitting. *Chem. Sci.* **2016**, *7*, 6076-6082, doi:10.1039/c6sc01611a.

51. D. Jiang; S. Zhang; H. Zhao. Photocatalytic Degradation Characteristics of Different Organic Compounds at TiO_2 Nanoporous Film Electrodes with Mixed Anatase/Rutile Phases. *Environ. Sci. Technol.* **2007**, *41*, 303-308, doi:10.1021/es061509i.
52. T. Ohno; K. Tokieda; S. Higashida; M. Matsumura. Synergism between rutile and anatase TiO_2 particles in photocatalytic oxidation of naphthalene. *Appl. Catal., A: Gen.* **2003**, *244*, 383-391.
53. K. L. Wang; Z. S. Wei; B. Ohtani; E. Kowalska. Interparticle electron transfer in methanol dehydrogenation on platinum-loaded titania particles prepared from P25. *Catal. Today* **2018**, *303*, 327-333, doi:10.1016/j.cattod.2017.08.046.
54. J. Zhang; P. Zhou; J. Liu; J. Yu. New understanding of the difference of photocatalytic activity among anatase, rutile and brookite TiO_2. *Phys. Chem. Chem. Phys.* **2014**, *16*, 20382-20386, doi:10.1039/c4cp02201g.
55. J. Nowotny. *Oxide Semiconductors for Solar Energy Conversion Titanium Dioxide*, 1st Edition ed.; Boca Raton, 2011, doi:10.1201/b11109.
56. D.A.H. Hanaor; C.C. Sorrell. Review of the anatase to rutile phase transformation. *J. Mater. Sci.* **2011**, *46*, 855–874, doi:10.1007/s10853-010-5113-0.
57. F. W. Zhang; L. Wang; C. P. Liu; P. Wu; S. Zhan. Patterns of convective flow in a vertically vibrated granular bed. *Phys. Lett. A* **2014**, *378*, 1303-1308, doi:10.1016/j.physleta.2014.03.001.
58. Y. C. Han; Q. L. Li; W. Liu; Y. J. He. Effect of Electromagnetic Vibration on the Agglomeration Behavior of Primary Silicon in Hypereutectic Al-Si Alloy. *Metall. Mater. Trans. A* **2012**, *43a*, 1400-1404, doi:10.1007/s11661-012-1130-8.
59. J. M. Valverde; A. Castellanos. Effect of vibration on agglomerate particulate fluidization. *Aiche J.* **2006**, *52*, 1705-1714, doi:10.1002/aic.10769.
60. V. Perera; A. P. Jackson; E. Asphaug; R. L. Ballouz. The spherical Brazil Nut Effect and its significance to asteroids. *Icarus* **2016**, *278*, 194-203, doi:10.1016/j.icarus.2016.06.014.
61. C. C. Liao; S. S. Hsiau. Transport Properties and Segregation Phenomena in Vibrating Granular Beds. *Kona Powder Part J* **2016**, 109-126.
62. M. E. Mobius; B. E. Lauderdale; S. R. Nagel; H. M. Jaeger. Size separation of granular particles. *Nature* **2001**, *414*, 270, doi:10.1038/35104697.
63. B. Ohtani; Y. Azuma; D. Li; T. Ihara; R. Abe. Isolation of anatase crystallites from anatase–rutile mixed particles by dissolution with hydrogen peroxide and ammonia. *Trans. Mater. Res. Soc. Jpn* **2007**, *32*, 401.
64. T. Ohno; K. Sarukawa; M. Matsumura. Photocatalytic activities of pure rutile particles isolated from TiO_2 powder by dissolving the anatase component in HF solution. *J. Phys. Chem. B* **2001**, *105*, 2417-2420, doi:10.1021/jp003211z.
65. A. Nitta; M. Takase; M. Takashima; N. Murakami; B. Ohtani. A fingerprint of metal-oxide powders: energy-resolved distribution of electron traps. *Chem. Commun.* **2016**, *52*, 12096-12099, doi:10.1039/c6cc04999k.

66. A. Nitta; M. Takashima; N. Murakami; M. Takase; B. Ohtani. Reversed double-beam photoacoustic spectroscopy of metal-oxide powders for estimation of their energy-resolved distribution of electron traps and electronic-band structure. *Electrochim. Acta* **2017**, doi:10.1016/j.electacta.2017.12.160.
67. E. Kowalska; O. O. Mahaney; R. Abe; B. Ohtani. Visible-light-induced photocatalysis through surface plasmon excitation of gold on titania surfaces. *Phys. Chem. Chem. Phys.* **2010**, *12*, 2344-2355, doi:10.1039/b917399d.
68. H. Kisch. On the problem of comparing rates or apparent quantum yields in heterogeneous photocatalysis. *Angew. Chem. Int. Ed.* **2010**, *49*, 9588-9589; author reply 9590-9581, doi:10.1002/anie.201002653.
69. E. Kowalska; S. Rau. Photoreactors for Wastewater Treatment: A Review. *Rec. Patent. Eng.* **2010**, *4*, 242-266, doi:10.2174/187221210794578583.
70. E. Kowalska; S. Rau; B. Ohtani. Plasmonic Titania Photocatalysts Active under UV and Visible-Light Irradiation: Influence of Gold Amount, Size, and Shape. *J. Nanotechnol.* **2012**, *2012*, 1-11, doi:Artn 361853/10.1155/2012/361853.
71. G. Chen; M. Takashima; B. Ohtani. Direct Amorphous-structure Analysis: How are Surface/Bulk Structure and Activity of Titania Photocatalyst Particles Changed by Milling? *Chem. Lett.* **2021**, *50*, 644-648, doi:10.1246/cl.200825.
72. A. Carati; C. Flego; E. P. Massara; R. Millini; L. Carluccio; W. O. Parker; G. Bellussi. Stability of Ti in MFI and Beta structures: a comparative study. *Microporous Mesoporous Mat.* **1999**, *30*, 137-144, doi:10.1016/S1387-1811(99)00018-9.
73. P. Wu; T. Komatsu; T. Yashima. Hydroxylation of Aromatics with Hydrogen Peroxide over Titanosilicates with MOR and MFI Structures: Effect of Ti Peroxo Species on the Diffusion and Hydroxylation Activity. *J. Phys. Chem. B* **1998**, *102*, 9297-9303, doi:10.1021/jp982951t.
74. D. Dolat; D. Moszynski; N. Guskos; B. Ohtani; A. W. Morawski. Preparation of photoactive nitrogen-doped rutile. *Appl. Surf. Sci.* **2013**, *266*, 410-419, doi:10.1016/j.apsusc.2012.12.048.
75. P. S. Yap; Y. L. Cheah; M. Srinivasan; T. T. Lim. Bimodal N-doped P25-TiO_2/AC composite: Preparation, characterization, physical stability, and synergistic adsorptive-solar photocatalytic removal of sulfamethazine. *Appl. Catal. A-Gen.* **2012**, *427*, 125-136, doi:10.1016/j.apcata.2012.03.042.
76. K. Wang; M. Janczarek; Z. Wei; T. Raja-Mogan; M. Endo-Kimura; T.M. Khedr; B. Ohtani; E. Kowalska. Morphology- and Crystalline Composition-Governed Activity of Titania-Based Photocatalysts: Overview and Perspective. *Catalysts* **2019**, 9(12), 1054, doi:10.3390/catal9121054.
77. B. Ohtani; Y. Ogawa; S. Nishimoto. Photocatalytic activity of amorphous-anatase mixture of titanium(IV) oxide particles suspended in aqueous solutions. *J. Phys. Chem. B* **1997**, *101*, 3746-3752, doi:10.1021/jp962702+.
78. J. M. G. Amores; V. S. Escribano; G. Busca. Anatase crystal growth and phase transformation to rutile in high-area TiO_2, MoO_3–TiO_2 and other TiO_2-supported oxide

catalytic systems. *J. Mater. Chem.* **1995**, *5*, 1245-1249, doi:10.1039/jm9950501245.
79. K. M. Reddy; S. V. Manorama; A. R. Reddy. Bandgap studies on anatase titanium dioxide nanoparticles. *Mater. Chem. Phys.* **2003**, *78*, 239-245.
80. S. Valencia; J. M. Marín; G. Restrepo. Study of the Bandgap of Synthesized Titanium Dioxide Nanoparticules Using the Sol-Gel Method and a Hydrothermal Treatment. *Open Mater. Sci.* **2010**, *4*, 9-14, doi:10.2174/1874088x01004010009.
81. R. A. P. Ribeiro; S. R. de Lazaro; C. R. de Oliveira. Band-Gap Engineering for Photocatalytic Applications: Anionic and Cationic Doping of TiO_2 Anatase. *Curr. Phys. Chem.* **2016**, *6*, 22-27.
82. M. Buchalska; M. Kobielusz; A. Matuszek; M. Pacia; S. Wojtyla; W. Macyk. On Oxygen Activation at Rutile- and Anatase-TiO_2. *ACS Catal* **2015**, *5*, 7424-7431, doi:10.1021/acscatal.5b01562.
83. M. V. Dozzi; E. Selli. Effects of the calcination temperature on the photoactivity of B- and F-doped or codoped TiO_2 in formic acid degradation. *Mater. Sci. Semicond. Process.* **2016**, *42*, 36-39, doi:10.1016/j.mssp.2015.08.007.
84. T. Khoa Le; D. Flahaut; D. Foix; S. Blanc; H. K. Hung Nguyen; T. K. Xuan Huynh; H. Martinez. Study of surface fluorination of photocatalytic TiO_2 by thermal shock method. *J. Solid State Chem.* **2012**, *187*, 300-308, doi:10.1016/j.jssc.2012.01.034.
85. U. Diebold. The surface science of titanium dioxide. *Surf. Sci. Rep.* **2003**, *48*, 53-229.
86. Z. Wei; E. Kowalska; B. Ohtani. Influence of post-treatment operations on structural properties and photocatalytic activity of octahedral anatase titania particles prepared by an ultrasonication-hydrothermal reaction. *Molecules* **2014**, *19*, 19573-19587, doi:10.3390/molecules191219573.
87. E. Kowalska; Z. Wei; B. Karabiyik; A. Herissan; M. Janczarek; M. Endo; A. Markowska-Szczupak; H. Remita; B. Ohtani. Silver-modified titania with enhanced photocatalytic and antimicrobial properties under UV and visible light irradiation. *Catal. Today* **2015**, *252*, 136-142, doi:10.1016/j.cattod.2014.10.038.
88. M. G. Mendez-Medrano; E. Kowalska; A. Lehoux; A. Herissan; B. Ohtani; D. Bahena; V. Briois; C. Colbeau-Justin; J. L. Rodriguez-Lopez; H. Remita. Surface Modification of TiO2 with Ag Nanoparticles and CuO Nanoclusters for Application in Photocatalysis. *J. Phys. Chem. C* **2016**, *120*, 5143-5154, doi:10.1021/acs.jpcc.5b10703.
89. D. O. Scanlon; C. W. Dunnill; J. Buckeridge; S. A. Shevlin; A. J. Logsdail; S. M. Woodley; C. R. Catlow; M. J. Powell; R. G. Palgrave; I. P. Parkin; et al. Band alignment of rutile and anatase TiO(2). *Nat. Mater.* **2013**, *12*, 798-801, doi:10.1038/nmat3697.
90. A. J. Bard. Photoelectrochemistry and heterogeneous photo-catalysis at semiconductors. *J. Photochem.* **1979**, *10*, 59-75, doi:10.1016/0047-2670(79)80037-4.
91. A. J. Bard. Photoelectrochemistry. *Science* **1980**, *207*, 139-144, doi:10.1126/science.207.4427.139.
92. R. Asahi; T. Morikawa; T. Ohwaki; K. Aoki; Y. Taga. Visible-light photocatalysis in nitrogen-doped titanium oxides. *Science* **2001**, *293*, 269-271, doi:10.1126/science.1061051.
93. C. Burda; Y. Lou; X. Chen; A. C. S. Samia; J. Stout; J. L. Gole. Enhanced Nitrogen Doping in TiO_2 Nanoparticles. *Nano Lett.* **2003**, *3*, 1049-1051, doi:10.1021/nl034332o.

94. O. Diwald; T. L. Thompson; T. Zubkov; E. G. Goralski; S. D. Walck; J. T. Yates. Photochemical activity of nitrogen-doped rutile TiO_2(111) in visible light. *J. Phys. Chem. B* **2004**, *108*, 6004-6008, doi:10.1021/jp031267y.
95. S. Sakthivel; M. Janczarek; H. Kisch. Visible light activity and photoelectrochemical properties of nitrogen-doped TiO_2. *J. Phys. Chem. B* **2004**, *108*, 19384-19387, doi:10.1021/jp046857q.
96. M. Barbeni; C. Minero; E. Pelizzetti; E. Borgarello; N. Serpone. Chemical degradation of chlorophenols with Fenton's reagent (Fe^{2+} + H_2O_2). *Chemosphere* **1987**, *16*, 2225-2237.
97. C. Randorn; J. T. S. Irvine; P. Robertson. Synthesis of Visible-Light-Activated Yellow AmorphousTiO_2 Photocatalyst. *Int. J. Photoenergy* **2008**, *2008*, 1-6, doi:10.1155/2008/426872.
98. X. S. Zhou; F. Peng; H. J. Wang; H. Yu; J. Yang. Preparation of nitrogen doped TiO2 photocatalyst by oxidation of titanium nitride with H_2O_2. *Mater. Res. Bull.* **2011**, *46*, 840-844, doi:10.1016/j.materresbull.2011.02.029.
99. W. F. Huang; P. Raghunath; M. C. Lin. Computational study on the reactions of H2O2 on TiO_2 anatase (101) and rutile (110) surfaces. *J. Comput. Chem.* **2011**, *32*, 1065-1081, doi:10.1002/jcc.21686.
100. M. N. Romanias; A. El Zein; Y. Bedjanian. Heterogeneous interaction of H2O2 with TiO2 surface under dark and UV light irradiation conditions. *J. Phys. Chem. A* **2012**, *116*, 8191-8200, doi:10.1021/jp305366v.
101. J. X. Zhao; W. T. Li; X. Li; X. K. Zhang. Low temperature synthesis of water dispersible F-doped TiO_2 nanorods with enhanced photocatalytic activity. *RSC Adv.* **2017**, *7*, 21547-21555, doi:10.1039/c7ra00850c.
102. M. Janczarek; E. Kowalska. Defective Dopant-Free TiO_2 as an Efficient Visible Light-Active Photocatalyst. *Catalysts* **2021**, *11*, doi:ARTN 97810.3390/catal11080978.